AGU PUBLICATIONS

JGR

Journal of Geophysical Research: Solid Earth

RESEARCH ARTICLE
10.1002/2016JB013272

Key Points:
- Determination of crustal stress field along a dense grid using 1614 focal mechanisms
- Minimum stress axes consistent with gravitational spreading of Aegean lithosphere
- Principal stress and strain axis orientations imply elastic behavior of the crust

Supporting Information:
- Supporting Information S1

Correspondence to:
K. I. Konstantinou,
kkonst@ncu.edu.tw

Citation:
Konstantinou, K. I., V. Mouslopoulou, W.-T. Liang, O. Heidbach, O. Oncken, and J. Suppe (2016), Present-day crustal stress field in Greece inferred from regional-scale damped inversion of earthquake focal mechanisms, *J. Geophys. Res. Solid Earth*, *121*, doi:10.1002/2016JB013272.

Received 13 JUN 2016
Accepted 26 NOV 2016
Accepted article online 6 DEC 2016

Present-day crustal stress field in Greece inferred from regional-scale damped inversion of earthquake focal mechanisms

K. I. Konstantinou[1], V. Mouslopoulou[2], W.-T. Liang[3], O. Heidbach[2], O. Oncken[2], and J. Suppe[4,5]

[1]Department of Earth Sciences, National Central University, Jhongli, Taiwan, [2]GeoForschungsZentrum, Potsdam, Germany, [3]Institute of Earth Sciences, Academia Sinica, Nankang, Taipei, Taiwan, [4]Department of Geosciences, National Taiwan University, Taipei, Taiwan, [5]Now at Department of Earth Sciences, University of Houston, Houston, Texas, USA

Abstract In this study we utilize regional and teleseismic earthquake moment tensor solutions in order to infer the contemporary crustal stress in the Greek region. We focus on crustal earthquakes and select only solutions with good waveform fits and well-resolved nodal planes. A data set of 1614 focal mechanisms is used as input to a regional-scale damped stress inversion algorithm over a grid whose node spacing is 0.35°. Several resolution and sensitivity tests are performed in order to ascertain the robustness of our results. Our findings show that for most of the Greek region the largest principal stress σ_1 is vertically oriented and that the minimum principal stress axis σ_3 are subhorizontal with a predominant N-S orientation. In the SW Peloponnese the orientation of σ_3 axes rotates clockwise and in SE Aegean counterclockwise. These results are in agreement with the generally accepted model that slab rollback combined with gravitational spreading of the Aegean lithosphere are the main causes of the extension. Transitions between different faulting types in NW Greece or in the Aegean occur within narrow zones in the order of tens of kilometers. A visual comparison of the principal horizontal stress axes and the principal strain axes derived from GPS observations shows good agreement, suggesting that the crust in the Greek region behaves largely in an elastic manner.

1. Introduction

Knowledge of the crustal stress field is a prerequisite for understanding the kinematics and distribution of continental deformation. This fact initiated three decades ago the creation of a database where stress data from a variety of sources worldwide would be gathered, leading to the compilation of the World Stress Map [*Zoback et al*., 1989; *Zoback*, 1992; *Sperner et al*., 2003; *Heidbach et al*., 2010]. The analysis of the compiled stress data showed that lithospheric stress is affected by processes that operate at distinctly different spatial scales [*Zoback*, 1992; *Heidbach et al*., 2007]. Forces that are related to plate motion (e.g., ridge push, slab pull, and trench suction) affect the larger wavelengths of the stress field (>2000 km), while lateral density contrasts and lithospheric flexure influence the stress field at intermediate wavelengths (2000–500 km) [*Zoback*, 1992; *Richardson*, 1992]. Active faulting, stress changes induced by earthquakes or volcanic eruptions, and local density contrasts tend to perturb the stress orientations produced by the aforementioned processes, creating small-scale (<100 km) stress field variations [*Pierdominici and Heidbach*, 2012; *Zoback*, 2010]. It is these variations that greatly influence the management of geothermal and hydrocarbon reservoirs [*Segall and Fitzgerald*, 1998; *Tingay et al*., 2005; *Fuchs and Müller*, 2001; *Martinez-Garzón et al*., 2013] as well as the nucleation sites of potentially destructive earthquakes [*Stein*, 1999; *Hergert and Heidbach*, 2011].

Stress can be derived from borehole breakouts, hydraulic fracturing and overcoring, or from volcanic vent alignments; however, the majority of stress data comes from seismological observations in the form of earthquake focal mechanisms. In theory, the *P* and the *T* axes of the focal mechanisms can be used as proxies for the orientation of the stress tensor [*McKenzie*, 1969; *Zoback*, 1992; *Célérier*, 2010]. In reality, prefracturing in the Earth's crust and friction along the fault surfaces makes this correspondence for a single focal mechanism less reliable. Thus, many methodologies have been proposed to derive the stress tensor from a set of focal mechanisms through inversion algorithms [*Gephart and Forsyth*, 1984; *Michael*, 1984, 1987; *Angelier*, 2002]; a review of which can be found in *Hardebeck and Hauksson* [2001] and in *Maury et al*. [2013]. The basic assumption of these methodologies is that the set of inverted focal mechanisms can be explained by one

stress tensor or in other words that stress is homogeneous. In order to fulfill this stress homogeneity requirement the study area is divided in smaller subareas, where stress complexity is assumed to be low, and separate inversions are performed in each of them. Any spatial stress changes from one subarea to the other may then be interpreted as a real feature or as an artifact created by the particular choice of subareas. In order to overcome this problem *Hardebeck and Michael* [2006] suggested an approach similar to the one followed in travel time tomography, namely, to perform a damped stress inversion along a regular grid of nodes covering the study area, where only the stress complexity that is strongly required by the data will be retained in the resulting stress field. The particular methodology has been applied to regions with complicated tectonics where spatial variations of stress are expected, such as Ryukyu-Taiwan-Luzon [*Wu et al*., 2010], Southern California [*Yang and Hauksson*, 2013], northern Turkey [*Ickrath et al*., 2014], and NE Japan [*Yoshida et al*., 2015].

The Greek region is a natural laboratory of tectonic processes that has been extensively studied in the past to better understand continental deformation. The dominant tectonic process along the Hellenic margin is the subduction of the African lithosphere beneath the Aegean plate at a rate of 0.9 cm/yr complemented by the southwestward movement of the Aegean plate at a rate of 3.5 cm/yr owing to slab rollback (Figure 1) [*McClusky et al*., 2000; *Kreemer and Chamot-Rooke*, 2004; *Nyst and Thatcher*, 2004; *Hollenstein et al*., 2008; *Reilinger et al*., 2010; *Rontogianni*, 2010; *Floyd et al*., 2010; *Jolivet et al*., 2013]. A consequence of the subduction is that a well-defined Wadati-Benioff zone can be traced in the southern Aegean along with a volcanic arc consisting of several active volcanoes [*Papazachos et al*., 2000]. The strongly curved shape of the subduction zone forms different angles with the motion vector of the African slab, imposing an increasing degree of obliqueness from the western to the eastern side [*Bohnhoff et al*., 2005]. Superimposed to the deformation related to the subduction and slab rollback is the westward movement of the Anatolian plate. Its motion is accommodated along the North Anatolian Fault (NAF), which traverses the northern part of Turkey, splaying into several branches as it extends offshore into the northern Aegean [*Koukouvelas and Aydin*, 2002; *Papanikolaou et al*., 2002]. On the other hand, western Greece is affected by the counterclockwise rotation of the Apulian plate that is accommodated by the Kefalonia Transform Fault (KTF) and its collision with the Eurasian margin [*Laigle et al*., 2002]. The end result of all these processes is high-seismicity levels throughout the Aegean and mainland Greece as well as the frequent occurrence of large ($M_w > 6$) earthquakes that occasionally cause damage and casualties [*Papazachos and Papazachou*, 2003].

Despite the fact that geodetic studies have resolved relatively well the strain field in the Aegean and mainland Greece, the crustal stress field is known in much less detail. Previously published studies derived present-day stress either by using *P* and *T* axes of earthquake focal mechanisms [e.g., *Hatzfeld et al*., 1990, 1995, 1999] or by inverting a limited number of earthquake focal mechanisms and obtaining the stress tensor for subjectively chosen subareas [*Kiratzi*, 2002; *Bohnhoff et al*., 2005; *Ganas et al*., 2005; *Tselentis et al*., 2006; *Konstantinou et al*., 2011; *Serpetsidaki et al*., 2012; *Friederich et al*., 2014]. In this work, we present new crustal stress data of unprecedented detail for Greece inferred from the inversion of 1614 earthquake focal mechanism solutions by using the method of *Hardebeck and Michael* [2006]. First, we give a brief description of the inversion methodology and also describe the selection process for the focal mechanism solutions. We then present the stress inversion results and their corresponding uncertainties, followed by several resolution and sensitivity tests for the purpose of assessing their robustness. Finally, we discuss the variability of the resulting stress field in the framework of regional tectonics and the previously derived surface strain field.

2. Data and Methodology

2.1. Selection of Earthquake Focal Mechanisms

Several research groups/agencies routinely determine deviatoric moment tensor solutions for the Greek region by inverting either teleseismic or regional waveform data. The National Observatory of Athens (NOA), Institute of Geodynamics, has been routinely inverting regional waveforms recorded by the Hellenic Unified Seismic Network and its predecessors, for the purpose of determining deviatoric moment tensors. For the period starting in early 2001 until late 2012 inversions were performed using the method of *Herrmann and Ammon* [2002] as implemented by *Konstantinou et al*. [2010]. After this period and until present moment tensors have been determined by using the ISOLA software package [*Sokos and Zahradnik*, 2008]. Before 2001 moment tensor solutions for earthquakes in Greece and surrounding regions were available from the Global Centroid Moment Tensor (GCMT; former Harvard CMT) group [*Ekström et al*., 2012, and

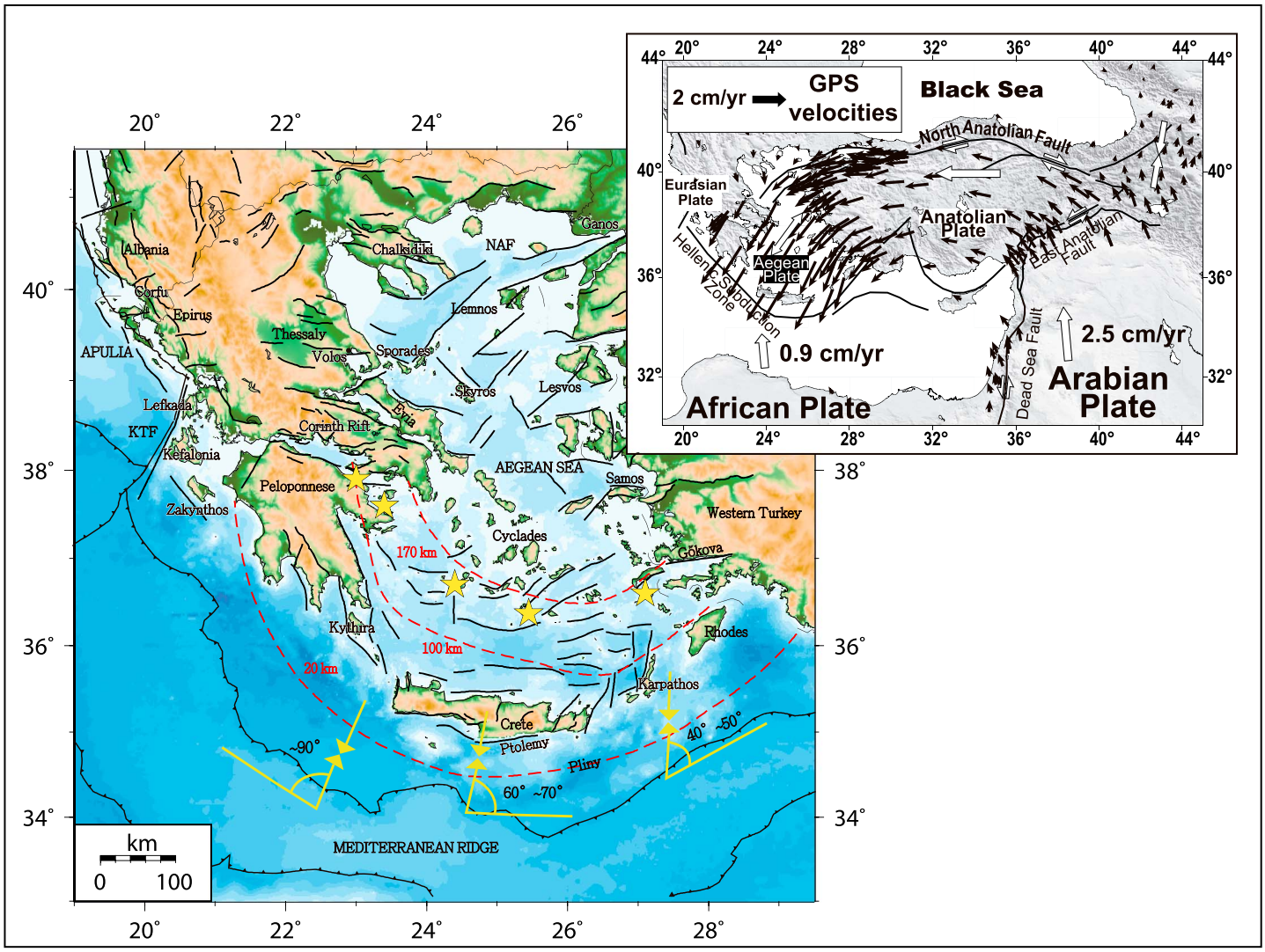

Figure 1. Map showing the main tectonic features of the Greek region and the surrounding areas. The black lines represent the active faults that have been extracted from the Greek Database of Seismogenic Sources (GREDASS) [*Caputo and Pavlides*, 2013]. The delineation of the Mediterranean Ridge has been adopted from *Chamot-Rooke and Dotmed Working Group* [2005]. The isodepth curves of 20, 100, and 170 km trace the hypocenters of earthquakes occurring along the Wadati-Benniof zone [*Papazachos et al*., 2000]. The yellow stars signify the locations of active volcanic centers. The yellow opposing arrows give the direction of motion for the African plate as determined from earthquake slip vectors [after *Bohnhoff et al*., 2005]. The direction of motion forms an angle with the strike of the subduction which systematically decreases from west to east. The inset map in the top right-hand corner shows the general geodynamic setting in the eastern Mediterranean. The thick white arrows represent the plate motions, and the black arrows indicate the GPS velocities relative to stable Eurasia [*Reilinger et al*., 2010]. The boundary between the Aegean and Anatolian plates is not shown, as it is still under debate.

references therein] and by the Regional CMT (RCMT) group based at Istituto Nazionale di Geofisica e Vulcanologia in Italy [*Pondrelli et al*., 2011, and references therein]. GCMT solutions have been produced since 1976 by inverting teleseismic body, surface, and mantle waves of earthquakes as small as M_w~5.0 worldwide. RCMT solutions are derived in a similar manner to those of GCMT; however, improved resolution of surface wave phase velocity maps allowed the application of the method to regional scale for smaller earthquakes (M_w~4.0). This methodology has been applied to earthquakes in the Mediterranean region since 1997 using waveform data recorded by the MEDNET seismic network.

We initially compiled a composite database of moment tensor solutions covering the periods between 1976 and 2000 (GCMT and RCMT solutions) and from 2001 to June 2015 (NOA solutions), paying particular attention on identifying solutions that existed in the two or even all three catalogs. Additionally, we searched through the published literature in order to find moment tensor solutions of events not existing in any of

the other three catalogs. Solutions from the literature were included in our database only when the misfit/variance reduction was given or plots of waveform fits were available. Table S1 in the supporting information that accompanies this paper gives details for each of the focal mechanisms included along with the corresponding reference it was obtained from. Even though numerous focal mechanisms derived from *P* wave polarities have been published over the years, we opted for not including these in our database. The reason for this decision was that we could not judge in an objective way the quality of such solutions, since many important factors were usually unknown (reliability of polarities, accuracy of takeoff angles, and other possible nodal plane solutions).

As a first step toward selecting suitable focal mechanisms for deciphering crustal stress, we included in the initial data set only events whose depth was less than 40 km. This was done by comparing hypocentral depths with the crustal thickness map that covers most of the Greek region and was derived from the modeling of receiver functions [*Sodoudi et al*., 2006]. It should be noted that all the selected events had two hypocentral depth values, namely, one adopted from the NOA earthquake location catalog and one determined by the depth-versus-misfit (or variance) curve of the moment tensor inversion. When there was a significant difference between the two values, the depth inferred from the moment tensor inversion was adopted as more reliable since inversions were performed using an interval of 2 km. We did not try to eliminate from our data set interplate events that mostly occur offshore southern Peloponnese and southern Crete, for the reason that they can provide clues about stresses related to the subduction process. Next we focused on the quality control of the CMT and NOA focal mechanisms, so as to reject any ill-constrained solutions. The solutions of the NOA data set have already a quality code assigned to them (from "A" as best quality to "D" as worst) based on the waveform misfit or variance reduction, while all of them are derived using data from at least three stations. We tightened further the quality control by requiring the stability of solutions around the depth where the misfit is minimum (or variance reduction is maximum) and that the nondouble-couple component is less than 50%. These requirements resulted in accepting the majority of quality A and B solutions along with a number of quality C solutions that satisfied our criteria and exhibited relatively good waveform fits. Representative examples of each category of solutions can be found in Figures S1–S5 in the supporting information accompanying this paper. The quality of the CMT data set has been studied by several authors previously [*Helffrich*, 1997; *Frohlich and Davis*, 1999; *Kagan*, 2003], who concluded that the contained uncertainty in the principal axes of the CMT solutions is on average 15°. Such an uncertainty is rather small and cannot bias significantly the results of our stress inversion; therefore, we chose to accept all CMT solutions for the Greek region prior to 2001. Nevertheless, we will further investigate the effect of CMT solutions on the stress inversion results in section 2.3, where we describe resolution and sensitivity tests.

The final data set consists of 1407 NOA solutions, 188 CMT solutions, and 19 solutions taken from the published literature, yielding a total of 1614 solutions covering a broad magnitude range (M_w~3.2–6.7). Figure 2 shows the distribution of these earthquakes in the form of event locations and their corresponding beach balls. It can be seen that the distribution is clearly not homogeneous with certain areas such as northern Greece, the Cyclades, and onshore Crete Island, lacking large enough earthquakes that could have been used for moment tensor inversion. The majority of the selected events have hypocentral depths that populate the first 15 km of the crust covering the northern Aegean, mainland, and western Greece. Events along the southern Aegean tend to occur at depths greater than 25 km as a result of seismicity near the plate interface.

2.2. Damped Stress Inversion

As mentioned earlier, the method of *Hardebeck and Michael* [2006] mimics seismic tomography algorithms by performing a damped inversion along a regular grid of nodes in order to determine the stress tensor at each node. A basic feature of this inversion is that it does a dual minimization: it minimizes the misfit between the stress tensor and the different focal mechanism solutions contained in each node, and at the same time, it minimizes any difference that may exist between stresses in adjacent nodes. The stress inversion at each node essentially follows the same method as the one described by *Michael* [1984] with an extra component added, which is the least squares damping that smoothes the differences in neighboring nodes. This approach effectively removes the problem of subjective choice of subareas and provides a more robust estimate of spatial stress changes than other commonly employed smoothing techniques.

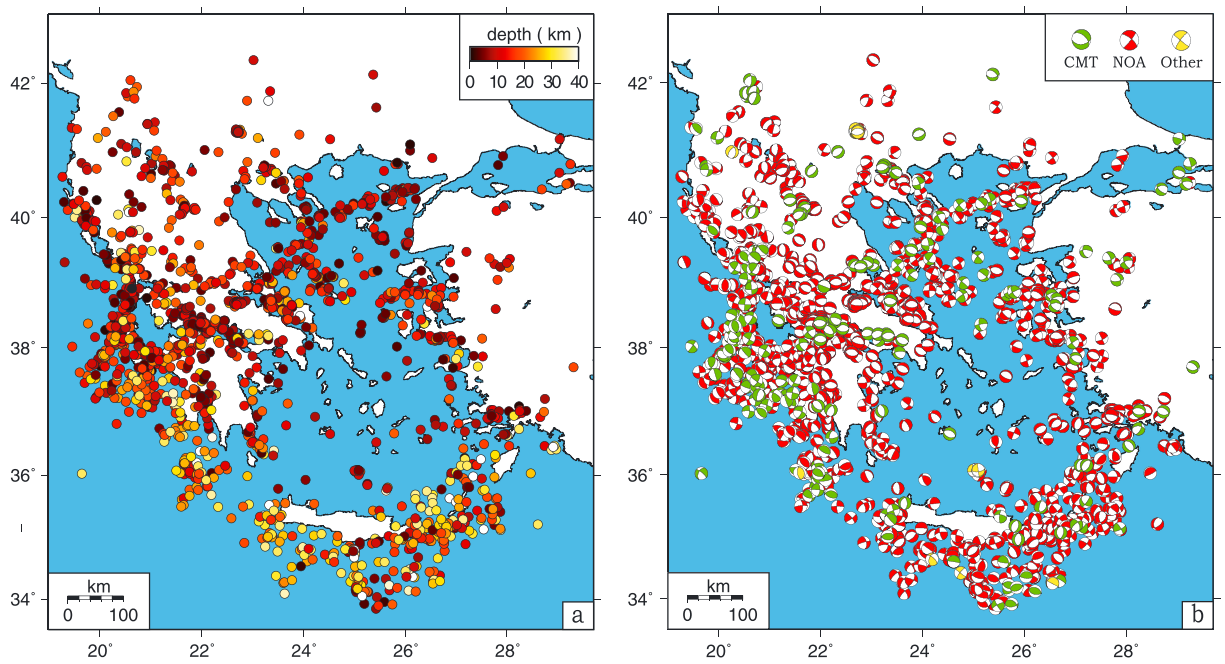

Figure 2. Summary of available earthquake observations that were used as input to the stress inversion. (a) Map of epicenters corresponding to crustal seismicity. The color of each circle varies according to the hypocentral depth of each event following the scale shown at the top right-hand corner of the plot. (b) Map of the beach balls of the 1614 earthquakes that have been utilized in this study. The color of the compressional quadrants of each beach ball signifies which database it belongs to, as shown in the legend at the top right-hand side corner of the plot.

The first parameter that should be set before applying this method is that of the grid spacing and for this study we choose a value of 0.35°. This is a compromise between finer node spacing that would have increased the computational load without providing any extra information about the stress field and coarser node spacing that would have concealed any spatial stress variations. We also set a requirement that at least eight focal mechanisms are located within one grid node spacing (~35 km) from each node in accordance with *Hardebeck and Michael* [2006]. In this way we obtained 249 nodes that contain 8 earthquakes or more, and Figure 3a depicts the spatial distribution of the number of earthquake counts at each node. It can be seen that 8–9 focal mechanisms occur in only 24 nodes (9.6% of the total number of nodes), while the average focal mechanisms per node is about 20. The next issue that should be investigated is whether the focal mechanisms in each node are diverse enough to obtain constrained orientations of the principal stress axes. In order to check this we estimated an average focal mechanism for each node and then calculated the angular difference (also known as "Kagan angle" [*Kagan*, 1991]) between the average and all the other solutions in that node. The root-mean-square (RMS) of these differences gives a good indication about the diversity of focal mechanisms in each node [see also *Wu et al.*, 2010, Figure 3b]. We excluded nodes from any further analysis when they exhibited an RMS value smaller than 40°, and this occurred in 15 nodes (about 6%). On the other hand, an RMS value of angular difference larger than 85° may indicate very diverse focal mechanisms that could be the result of stress heterogeneity, in which case stress inversion results in these nodes should be viewed with caution.

The last parameter that should be set before applying the stress inversion is that of the damping value, which determines the trade-off between the fit of the model to the data and the degree of model smoothness. This trade-off can be expressed in a diagram of data variance versus model length, where data variance represents the difference between the data and what is predicted by the model, while model length represents the difference between stress tensors at neighboring nodes. We performed a series of trial inversions using damping values in the range of 0.02–50 in order to compute the curve that describes this trade-off (Figure 4). A damping value of 1.6 is then chosen as a compromise between large model lengths with small data variance and small model lengths with large data variance. The results of the damped stress inversion can be seen in Figure 5 in terms of the azimuth and plunge of the maximum (σ_1) and minimum (σ_3) principal

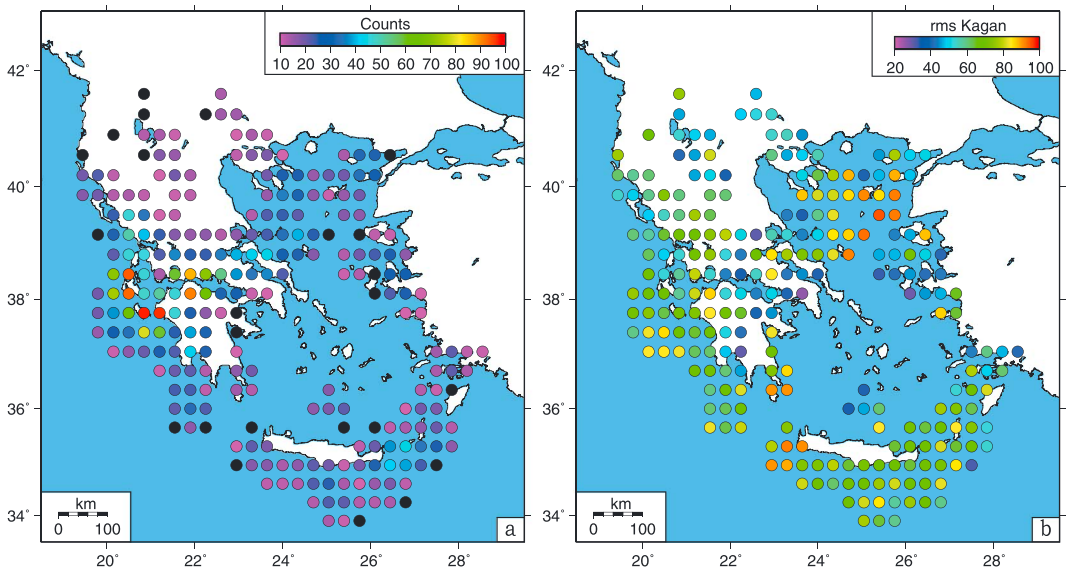

Figure 3. Maps showing the grid nodes signified by circles that contained at least eight focal mechanisms along with the variation of two quantities. (a) The number of focal mechanisms per node, where the color of each circle follows the scale at the top right-hand corner. The black circles represent the nodes that have eight or nine focal mechanisms. (b) The root-mean-square Kagan angle difference for each node that measures faulting diversity (see text for more details). The color of each circle follows the scale shown at the top right-hand side corner of the plot.

stress axes (where $\sigma_1 > \sigma_2 > \sigma_3$). Uncertainties have been estimated using 2000 bootstrap resamplings of the data corresponding to a confidence level of 95% [e.g., *Hardebeck and Hauksson*, 2001]. The inversion also determines for each node the dimensionless parameter $\Phi = (\sigma_2 - \sigma_3)/(\sigma_1 - \sigma_3)$, which represents the ratio of stress differences and takes values in the interval of 0–1. However, *Vavryčuk* [2014] used synthetic as well as observed data in order to show that the linear inversion method of *Michael* [1984, 1987] produces biased estimates of Φ (with an error of 20% or higher) in the case when fault and auxiliary planes are not correctly identified. For this reason we do not make use of the ratio Φ in our subsequent interpretations and only include a map of its spatial distribution in Figure S6.

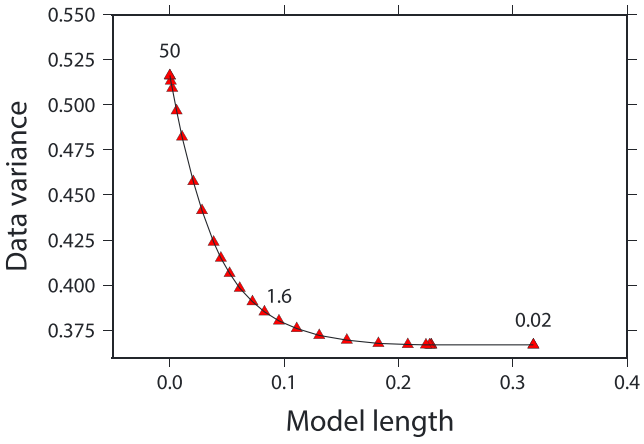

Figure 4. Diagram showing the variation of data variance versus model length as a means to infer the proper damping value for the stress inversion. The red triangles represent the results for damping values in the range of 0.02–50, and the chosen value of 1.6 is highlighted in the diagram. The model length axis has been shifted to the right for clarity.

2.3. Resolution, Sensitivity, and Robustness of Results

One way to validate the results of the damped stress inversion is by performing a resolution test very similar to checkerboard tests used in seismic tomography. Following *Hardebeck and Michael* [2006], we created a synthetic data set where the maximum principal stress alternates its orientation from N-S to N45°E in blocks that have a size of 1°×1° also assuming that $\Phi = 0.5$ (i.e., σ_1 and σ_3 axes are horizontal with σ_2 vertical, which is a strike-slip stress regime). We used our original data set as the basis of the synthetic one, in the sense that locations as well as selected nodal planes are the same. The rake of the nodal plane is switched to the direction of resolved shear stress (N-S or N45°E), depending on which block

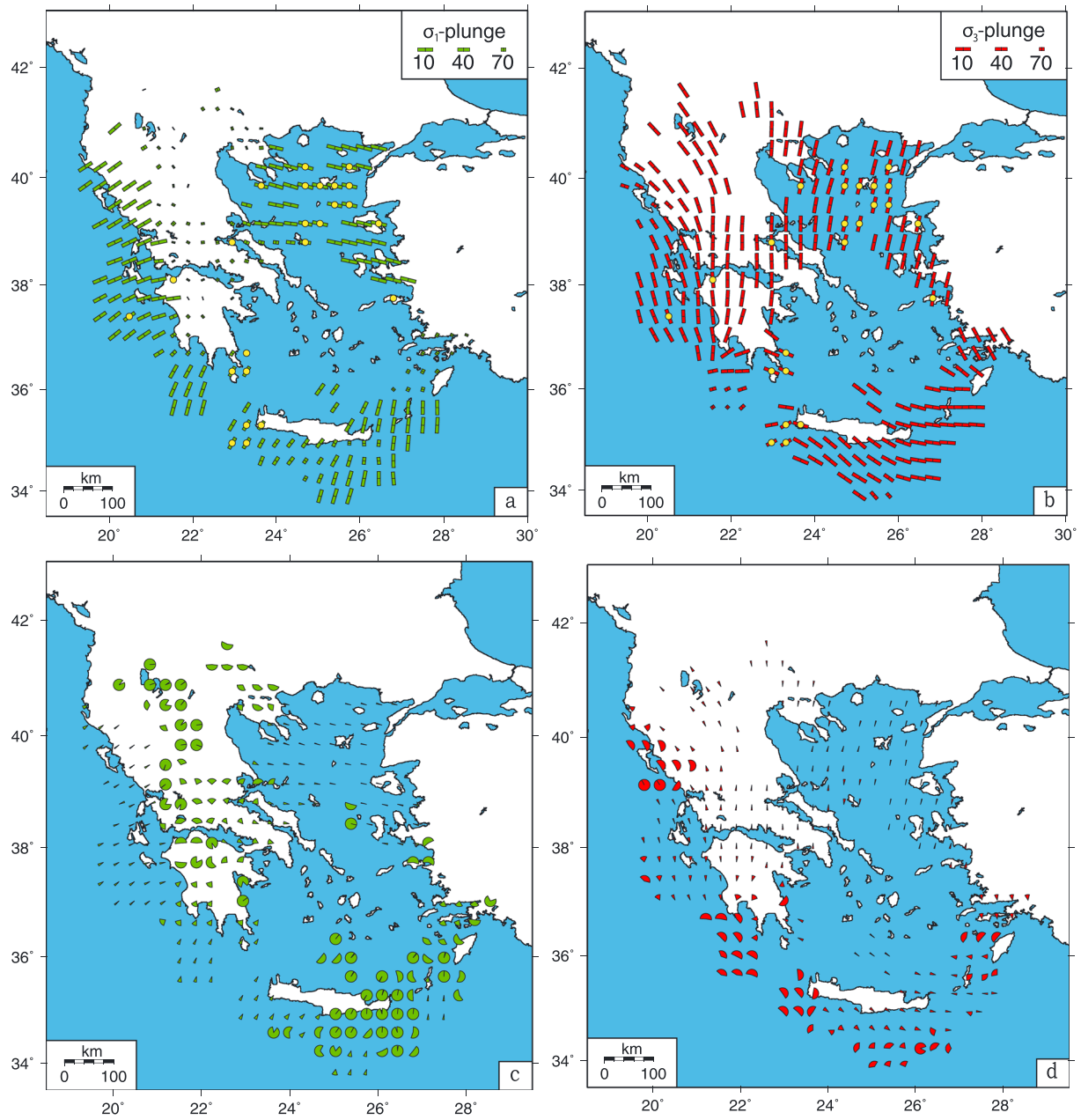

Figure 5. Maps summarizing the results of the application of the stress inversion methodology of *Hardebeck and Michael* [2006] to the Greek region: (a) spatial distribution of azimuth and plunge for principal maximum stress axes. The length of each axis varies according to its plunge angle, following the scale shown at the top right-hand corner of the plot. The yellow circles plotted at some of the nodes highlight the presence of increased faulting diversity that may imply stress heterogeneity. (b) The same for principal minimum stress axes, (c) 95% bootstrap uncertainty results for the maximum stress axes, and (d) the same for the minimum stress axes.

the earthquake belongs to. We performed two inversions: one in which a random error with a standard deviation of 30° is added to the strike, dip, and rake and another with no added error. The results are shown in Figures S7 and S8. In both cases the checkerboard stress pattern is to a good extent recovered, allowing us to conclude that the application of the damped inversion methodology to our data can indeed resolve spatial variations of stress.

Damping, grid node spacing, and the number of solutions per node may influence the results of the stress inversion, and the effect of changing any of these was investigated in a series of sensitivity tests. First, we checked whether our results depend in any way on the particular choice of damping value we used.

Several trial inversions were performed with distinctly different damping values, and the principal stress axis orientations were compared with the ones obtained previously. This test showed that a variation of the damping value in the range of 1.1–2.1 does not alter our results for the majority of the nodes (Figure S9). The second test has to do with the grid node spacing and how results may change when its value becomes coarser or finer than 0.35°. We performed two inversions, one with a grid spacing of 0.2° and another with 0.5° node spacing, both producing almost identical results to those with 0.35° spacing (Figures S10 and S11). Even though there is no general consensus about the minimum number of focal mechanisms required for a constrained stress inversion, one could argue that results from nodes containing only 8–12 focal mechanisms are not well constrained. The number of available focal mechanism solutions at each grid node is directly related to the maximum distance that a solution is allowed to lie from the node. We therefore increased the maximum allowed distance from 35 to 53 km (an increase by a factor of 1.5) and repeated the inversion by requiring that at least 16 solutions are available per grid node. Figure S12 shows a comparison between results for these two maximum distances, where it can be seen that azimuths and plunges of the stress axes are almost the same.

The next series of sensitivity tests investigates whether changes in the composition of the data set have any effect on the stress inversion results. The data set was first divided into two subsets based on the hypocentral depth of the earthquakes: a subset consisting of events that occurred at 15 km or shallower and one subset with all the deeper events. The value of 15 km was chosen as it is comparable to the average thickness of the seismogenic layer in the Greek region [see *Konstantinou*, 2014]. Subsequently, inversions were performed for the two subsets and the results were compared showing very little variation between the shallow and deeper seismicities (Figure S13). It can also be argued that our results may be sensitive to the magnitude of the earthquakes used in the inversion, since larger earthquakes reflect large-scale stress variations while smaller ones are usually related to localized stress patterns. We performed separate inversions for a subset consisting of all events with $M_w \leq 4.5$ and another subset with all events with M_w larger than 4.5. We again find a very good agreement between the results of the two inversions and our original results that were based on the whole data set (Figure S14). Finally, we investigated how our results would change if we exclude from the inversion all CMT focal mechanism solutions. The comparison of the original results with those without the CMT solutions exhibit insignificant changes for the majority of the nodes (Figure S15).

3. Description of Stress Inversion Results

3.1. Southern Aegean

The subduction of the African slab beneath the Aegean plate in its western part extends from south of Zakynthos Island, continuing in a SE direction toward western Crete (cf. Figure 1). *Shaw and Jackson* [2010] found that thrust focal mechanisms along the western part of the subduction belong to two distinct groups. The first group occurs at depths greater than 20 km (down to a maximum depth of 40 km), the dip of the fault planes ranges between 10° and 25°, and they represent typical interplate earthquakes. The second group occurs at shallower depths (<20 km); it exhibits fault plane dips of 30° or more and is probably the manifestation of a fault splaying from the plate interface in the upper plate. This splay fault is partly responsible for the uplift of the western Crete shoreline and is thought to be the source of the megathrust earthquake and tsunami in 365 A.D. and other similar earthquakes during the last 50 kyr [*Shaw et al*., 2008; *Stiros*, 2010; *Mouslopoulou et al*., 2015]. In this framework, the horizontal σ_1 axes offshore SW Peloponnese with NNE to NE-SW directions indicate the compression of the upper plate owing to the northward subduction of the African lithosphere. The σ_3 axes are less well constrained as judged by the bootstrap uncertainties; however, in southern Peloponnese and western Crete they attain a horizontal E-W or ENE-WSW orientation, which is consistent with previous geological and seismological observations that suggest along-arc extension [*Angelier et al*., 1982; *Lyon-Caen et al*., 1988; *Benetatos et al*., 2004].

The morphology of the offshore area south of Crete is characterized by the Ptolemy and Pliny troughs that exhibit a NE-SW orientation (cf. Figure 1), forming the tips of steep reverse seismogenic faults that splay off the plate interface [*Shaw and Jackson*, 2010; *Kokinou et al*., 2012; *Mouslopoulou et al*., 2015]. These structures accommodate also an amount of left-lateral slip owing to the progressive obliqueness of the subduction [*Huguen et al*., 2001; *Bohnhoff et al*., 2005]. The seismicity in this area has been studied relatively well using temporary seismic networks installed onshore Crete and also ocean bottom seismometers placed

offshore [*Meier et al*., 2004; *Becker et al*., 2006, 2010]. While onshore Crete earthquakes have hypocentral depths of 20 km or shallower, their depth is increasing southward as most of the seismicity occurs between 30 and 40 km along the plate interface. The seismicity is observed to form well-defined clusters along the Ptolemy trough, becoming more diffuse in the east toward the Pliny trough. Our stress inversion results for this area indicate that the σ_1 axes are orientated N or NNE, with plunges that in most cases exceed 40°, suggesting a rather extensional stress regime (cf. Figure 5). This is confirmed by the almost horizontal σ_3 axes that are orientated NW-SE and that are progressively rotating counterclockwise to E-W as we move from eastern Crete to the area around Karpathos Island. It is obvious therefore that the increasingly oblique movement of the African lithosphere along with the slab rollback impose a transtensional stress regime in the upper plate south of Crete. Further to the NE the minimum principal stress axes rotate clockwise back to NW-SE near Rhodes, while the σ_1 axes progressively become steeper until they attain subvertical plunge angles in the Gökova graben in SW Turkey.

The Sea of Crete is a largely aseismic sedimentary basin that is bordered by the eastern coast of Peloponnese, Crete Island to the south, the Cyclades to the north, and Karpathos and Rhodes Islands to the east. In January 2012 two moderate size events (M_w~5.0–5.3) occurred to the south of Santorini Island and were accompanied by a swarm of smaller-magnitude earthquakes over the next few weeks. The located events had hypocentral depths in the range of 5–14 km, and the moment tensor solutions of the largest of them showed strike-slip faulting [*Kiratzi*, 2013]. The swarm occurred immediately after the cessation of unrest in Santorini caldera that had started a year earlier and was characterized by intense seismicity and vertical/radial deformation [see *Konstantinou et al*., 2013, and references therein]. The temporal proximity of the caldera unrest and the swarm suggests a possible triggering effect that was subsequently confirmed through Coulomb stress modeling [*Feuillet*, 2013; *Saltogianni et al*., 2014]. Despite the transient nature of the swarm in the Sea of Crete, its generation provided us with the opportunity to probe into the stress regime in this aseismic part of the southern Aegean. Three nodes had enough focal mechanism solutions to invert for the stress tensor, revealing horizontal minimum stress axes with orientation almost parallel to those south of Crete (NW-SE; cf. Figure 5). Such an observation provides evidence that the stress north of Crete is influenced by the oblique subduction and slab rollback as the area to the south.

Two other studies had previously attempted to invert focal mechanism solutions in order to determine stress tensors for different areas in the southern Aegean. *Bohnhoff et al*. [2005] used 264 fault plane solutions, the majority of which have been estimated using *P* wave polarities, in order to derive stress tensors for the area around Crete and Karpathos Islands. The eight subareas they used for obtaining individual stress tensors had dimensions ranging from 50 to 100 km, much coarser than the 35 km of our nodes spacing. Their results are broadly similar to ours except from small differences in the orientation and plunge of the stress axes, which is reasonable considering that they obtained only a gross average of the stress field in each subarea. More recently, *Friederich et al*. [2014] utilized data recorded by the temporary CYCNET/EGELADOS seismic networks and estimated moment tensors for few larger events while producing solutions using *P* wave polarities for the numerous smaller ones. Their strategy was to identify clusters of seismicity in the southern Aegean and then invert all focal mechanisms within each cluster for deriving the stress tensor. This approach avoids the explicit delineation of subareas and identifies small areas where the assumption of stress homogeneity is likely to hold true. We can compare our results with those of *Friederich et al*. [2014] only for the areas of Karpathos Island and the Gökova graben, since all the other clusters they used lie in the Cyclades, where we do not have any earthquakes in our data set. While there is agreement about the change of plunge for the maximum stress axis from horizontal in the south to subvertical north of Karpathos, we observe a significant difference in the azimuth (~N147°E) when compared to our results (~N10°E). Likewise, their minimum stress axis appears with a NE-SW orientation, while ours has a E-W orientation. In the Gökova graben we observe differences in both the azimuth (N-S versus our NE-SW for σ_1 and NNE-SSW versus our NW-SE for σ_3) and plunge (~52° versus our ~70° for σ_1 and ~38° versus our ~10° for σ_3). We attribute these differences to the fact that their use of clustered microearthquakes probably resulted in deriving the local rather than the regional stress field.

3.2. Northern and Central Aegean

The westward movement of the Anatolian plate is achieved through the dextral strike-slip North Anatolian Fault (NAF) that splays into several branches in the northern Aegean, the largest of which extends from

Ganos Gulf to the Sporades Islands [*Koukouvelas and Aydin*, 2002; *Papanikolaou et al*., 2002]. The shearing deformation resulting from this process is superimposed to the extensional deformation related to slab rollback giving rise to a rather complex stress field [*Flerit et al*., 2004; *Kreemer et al*., 2004]. This is supported by seismic reflection profiles that reveal the main shearing zones and secondary normal faults that provide evidence for transtensional deformation [*Saatçilar et al*., 1999; *Laigle et al*., 2000]. Even though the seismicity in this area has not been studied in detail, most earthquakes are shallow (<20 km) and occur along the main branches of NAF with a smaller percentage occurring in between [*Kiratzi*, 2002; *Ganas et al*., 2005; *Evangelidis*, 2015].

Our stress inversion results show a very uniform distribution of the maximum stress axes with WNW-ESE azimuths and small plunge angles over most of northern Aegean. This trend changes south of latitude 38°, where the plunges become close to vertical at Samos Island, indicating the waning of the shearing deformation owing to NAF and the dominance of pure normal faulting (cf. Figure 5). On the other hand, the minimum stress axes are orientated also uniformly along the NNE-SSW direction and are almost horizontal as well. However, this rather simple pattern should be viewed with caution, since several of the nodes exhibit significant faulting diversity as attested by the high values of the RMS Kagan angle difference (cf. Figure 3). Most of these nodes actually fall between the main branches of NAF and give a hint of increased stress complexity. *Chatzipetros et al*. [2013] have also identified on the nearby islands of Lemnos and Lesvos a variety of faulting styles that seem to coexist with the main shearing fault zones. The authors suggest that in areas adjacent to large shearing zones (such as NAF), the deformation tends to follow a local fracture pattern. These observations of surface faulting traces indicate that smaller strike-slip faults may form at a variable angle to the main shearing zone, while normal faults may also form perpendicular to the σ_3 axes. In this case the resulting focal mechanisms will exhibit significant diversity as the one we observed.

A previous study that performed stress inversion of earthquake focal mechanisms in this area has been published by *Kiratzi* [2002]. At the time of that study, relatively few moment tensor solutions were available; therefore, only 18 were used in order to obtain a single stress tensor for the entire northern Aegean. Despite the lack of sufficient data the stress tensor is very similar to our results for both the maximum stress axis (azimuth N274°E, plunge 4°) and the minimum stress axis (azimuth N4°E, plunge 5°). Obviously, these results give no hint of stress heterogeneity, all the more since the angular misfit of the stress inversion reported by *Kiratzi* [2002] is low (~5.2°). Such a contradiction, however, can be easily explained if we take into account that the focal mechanisms utilized by *Kiratzi* [2002] mostly included GCMT solutions of large events that represented strike-slip faulting along the main branches of NAF. On the other hand, *Ganas et al*. [2005] used aftershocks of the 2001 (M_w 6.4) Skyros earthquake to determine focal mechanisms utilizing *P* wave polarities and derived one stress tensor for the central Aegean, obtaining maximum stress axis (azimuth N282°E, plunge 9°) and minimum stress axis (azimuth N13°E, plunge 7°) that are very close to our inferred orientations.

3.3. Mainland Greece

Geological, geodetic, and seismological observations have been utilized in order to identify the major fault zones traversing mainland Greece and understanding their kinematics [*Rigo et al*., 1996; *Hatzfeld et al*., 1999, 2000; *Goldsworthy et al*., 2002; *Shaw and Jackson*, 2010; *Mouslopoulou et al*., 2014; *Chousianitis et al*., 2015]. Normal faults with E-W orientation prevail in central Greece up to a latitude of about 39° accommodating the opening of three rifts, namely, the Gulfs of Corinth, Evia, and Volos. Further north, normal faulting changes strike to take a NE-SW direction to become again E-W in the Chalkidiki peninsula. Our stress inversion results for mainland Greece depict quite well this pattern with close to vertical σ_1 axes and minimum stress axes that change from NW-SE in the north to almost N-S in central Greece and northern Peloponnese. Recently, *Giannopoulos et al*. [2015] have conducted a study of crustal shear wave anisotropy in the western part of the Corinth Gulf and found that fast directions (corresponding to maximum horizontal stress σ_{Hmax}) have azimuths in the range of N68°E to N125°E. This is in good agreement with our stress inversion results for the azimuth of σ_2 stress axes around the same area. To the best of our knowledge, there is no study performing stress inversion in a systematic way in central or northern Greece, except from *Kiratzi* [2002] that inverted focal mechanisms in eastern Thessaly and northern Evia. We have good agreement for the areas of eastern Thessaly with maximum stress axes subvertical (58°–75°) and minimum stress axes with

azimuths N359°E and N186°E, while their plunge is close to horizontal (15°–29°). In northern Evia on the other hand, both axes are close to horizontal, while our results place σ_1 as subvertical.

3.4. Western Greece and Southwestern Albania

The dominant tectonic feature in western Greece is KTF that extends offshore, parallel to the west coasts of Lefkada and Kefalonia, up to a point west of Zakynthos Island [*Clément et al*., 2000; *Kokinou et al*., 2005, 2006] (cf. Figure 1). KTF consists of at least two segments and essentially divides the area into two parts: the one where continental collision takes place along Epirus/SW Albania and the one in the south where the subduction of the African slab takes place near Zakynthos [e.g., *Clément et al*., 2000]. Western Greece exhibits also two other notable features: a series of Quaternary grabens all of them bounded by active normal faults [*Ferentinos et al*., 1985; *Hatzfeld et al*., 1995; *Evangelidis et al*., 2008] and the occurrence of Triassic evaporites that may perturb locally the regional stress field and also influence the location and rupture extent of earthquakes in the area [*Melis and Tselentis*, 1998; *Tselentis et al*., 2006]. Seismicity that occurs around KTF represents either pure strike-slip faulting or some additional component of thrust faulting. Based on analysis of gravity observations, *Shaw and Jackson* [2010] suggested that the elastic part of the Ionian Sea lithosphere is flexed owing to the SW motion along KTF, which may explain the presence of a thrust component. Along Epirus and southern Albania low-angle thrust faulting dominates as a result of the continent-continent collision [*Hatzfeld et al*., 1995; *Tselentis et al*., 2006; *Serpetsidaki et al*., 2012]. To the south of Zakynthos low-angle thrust faulting occurs at the shallow dipping interface of the subduction. On the other hand, the seismicity in NW Peloponnese corresponds to pure strike-slip faulting as a result of its rotation owing to the opening of the Corinth Gulf [*Baker et al*., 1997; *Laigle et al*., 2002; *Konstantinou et al*., 2009, 2011].

Almost all the nodes covering the area of western Greece contain a minimum of 20 focal mechanisms, with the majority of them containing on average 40 and a few nodes more than 90 (cf. Figure 3a). Such a high-density distribution of focal mechanisms resulted in both the maximum and minimum stress axes to be well constrained for most of the nodes. The RMS Kagan angles are also within the stress homogeneity window we set earlier for the majority of the nodes (cf. Figure 3b). From southern Albania to the south of Zakynthos Island, stress inversion results clearly show horizontal σ_1 axes with an almost uniform NE-SW azimuth representing compression of the upper plate either owing to continental collision in the north or subduction of the African slab in the south (cf. Figure 5). Minimum stress axes do not exhibit this degree of uniformity; rather, in the north some nodes along the coast of Epirus and SW Albania seem to have subvertical σ_3 reflecting continental collision thrusting, while their azimuths are not well constrained. The plunge of the σ_3 axes decreases southward, and the azimuths change to NNW-SSE even though there are small variations from node to node. Two nodes, one in NW Peloponnese and another offshore SW Zakynthos, also exhibit faulting diversity above the threshold we have set, implying stress heterogeneity. While for the latter node the reasons for the heterogeneity are not clear, the former node lies at the edge of the rupture zone of the 8 June 2008 (M_w~6.4) earthquake [e.g., *Konstantinou et al*., 2009, 2011]. Analysis of the rich aftershock sequence, in terms of precise hypocenter locations and focal mechanisms, revealed that while the main part of the rupture represented a NE-SW orientated strike-slip fault, its NE edge exhibited a mixture of faulting styles [*Serpetsidaki et al*., 2014]. This probably explains the observed large RMS Kagan angle difference in that node and hence the implied stress heterogeneity.

Unlike other areas in the Greek region, a series of studies have performed stress inversions in western Greece using seismological observations recorded by temporary networks. *Tselentis et al*. [2006] studied the seismicity in Epirus using a dense temporary network and calculated 434 focal mechanisms of microearthquakes from *P* wave polarities that were subsequently used for stress inversion. Their results indicate azimuths and plunges of maximum/minimum stress axes compatible with the ones presented here for two of the three subareas chosen. Taking into account that most of the earthquakes the authors used were actually smaller than magnitude 3.0, we conclude that any differences reflect the influence of local stresses. *Serpetsidaki et al*. [2012] repeated the same analysis in SW Albania, using again a temporary seismic network of 40 stations but a much larger data set (~810 solutions). This time the stress inversion results in all six subareas are in general consistent with ours, both for σ_1 axes (azimuths from N62°E to N233°E, plunges 3°–30°) and σ_3 axes (azimuths from N91°E to N318°E). In NW Peloponnese *Konstantinou et al*. [2011] determined one stress tensor using GCMT and NOA solutions (a smaller sample of what is used in this study), obtaining almost the same stress axes as here.

4. Discussion

To understand which are the key forces that cause the distribution of crustal stress in the Greek region *Meijer and Wortel* [1997] conducted a series of 2-D geomechanical-numerical models. They considered two kinds of forces exerted on the western (Peloponnese, western Crete) and eastern (Karpathos, Rhodes) Hellenic subduction margin (cf. Figure 1): extensional (pull) forces orientated normal to the margin owing to the slab rollback and a much smaller force owing to the resistance of the convergence along the trench. To these forces they also superimposed a force that is related to the westward movement of the Anatolian plate. At this point it should be noted that *Meijer and Wortel* [1997] did not explicitly consider the resistance force from continental collision in NW Greece in their model, but rather, they assumed this segment to be blocked. This combination of forces provided the closest match between their model results and stress observations available to them at that time. In particular, their results showed N-S orientation of minimum stress axes north of latitude 38°, progressively rotating clockwise in southern Peloponnese and counterclockwise around Karpathos and Rhodes with decreasing distance from the trench. The inclusion of the resistance force had the effect of changing the orientation of some minimum stress axes to NW-SE orientation. Our stress inversion results in the southern Aegean show good agreement with this force configuration and the rotation of the σ_3 axes toward the trench in the western and eastern sides of the subduction. The NW-SE orientation of some nodes close to Kythira Island and SE Peloponnese is also in accordance with the convergence resistance force in the numerical simulations; however, the presence of stress heterogeneity in these nodes (cf. Figure 5) makes this assertion less certain. The stress field in the northern Aegean is the result of two superimposed effects: primarily N-S or NNE-SSW tension owing to slab rollback and additional E-W compression owing to the western push of the Anatolian plate. Again, our stress inversion results for the northern Aegean confirm the key findings of the numerical simulations and also provide more details on the local stress heterogeneity caused by the complex tectonic setting of this area.

The widespread extension in the Aegean region, highlighted also by our stress inversion results, has been attributed by many authors to gravitational spreading of the upper plate [e.g., *Hatzfeld et al*., 1997; *Martinod et al*., 2000; *England*, 2003]. Gravitational spreading is a direct consequence of slab rollback where the looser contact between the upper and subducting plate allows the seaward movement of the overriding lithosphere resulting in extension. This extension is believed to have been ongoing since Oligocene times probably having occurred in two episodes: one during Oligo-Miocene and a second one that started in the Plio-Pleistocene [see *Gautier et al*., 1999]. Inversion of marine gravity data showed that the Moho topography in the Aegean is relatively flat [*Tirel et al*., 2004] and suggested that extension affected the whole of the crust, a conclusion also supported by our results of a similar stress field for different earthquake depth intervals. An interesting question then is how our results compare with stress indicators of these earlier geological periods. *Doutsos and Kokkalas* [2001] compiled 900 slip measurements from striations on faults bounding postmiddle Miocene basins in mainland Greece and the southern Aegean. This data set was used to obtain palaeostress tensors utilizing graphical methods and direct inversion. We observe good agreement of their tension directions with the orientation of our minimum stress axes, especially for faults of Plio-Quaternary/Plio-Pleistocene age (Figure 6). The authors also interpreted their results as indicating extension caused by pull forces exerted at the subduction margins. This leads us to the conclusion that crustal stress in mainland Greece and the southern Aegean did not change much from the Plio-Quaternary/Plio-Pleistocene until present.

As mentioned earlier, the surface strain field is relatively well known for the Greek region; therefore, it is possible to compare it with our stress inversion results. The most recent study of such kind was published by *Floyd et al*. [2010], and in Figure 7, we visually compare the azimuths of the principal stress and strain axes. It can be seen that with the exception of minor rotations of the extensional axes or areas where there are no strain estimates, the stress and strain fields correlate well with each other. This good agreement between stress and strain orientations can be interpreted as an indication that the crust behaves, at least to some extent, in an elastic manner in the Aegean and mainland Greece. This in turn means that the deformation process responsible for the earthquakes is also responsible for the surface strain field as found in other areas worldwide such as Taiwan [*Chang et al*., 2003], Iceland [*Keiding et al*., 2009], and Italy [*Palano*, 2015]. *Floyd et al*. [2010] also observed a relationship between the extensional strain axes and the strike of major normal or strike-slip faults in the sense that normal faults were perpendicular to the axes, while strike-slip faults formed

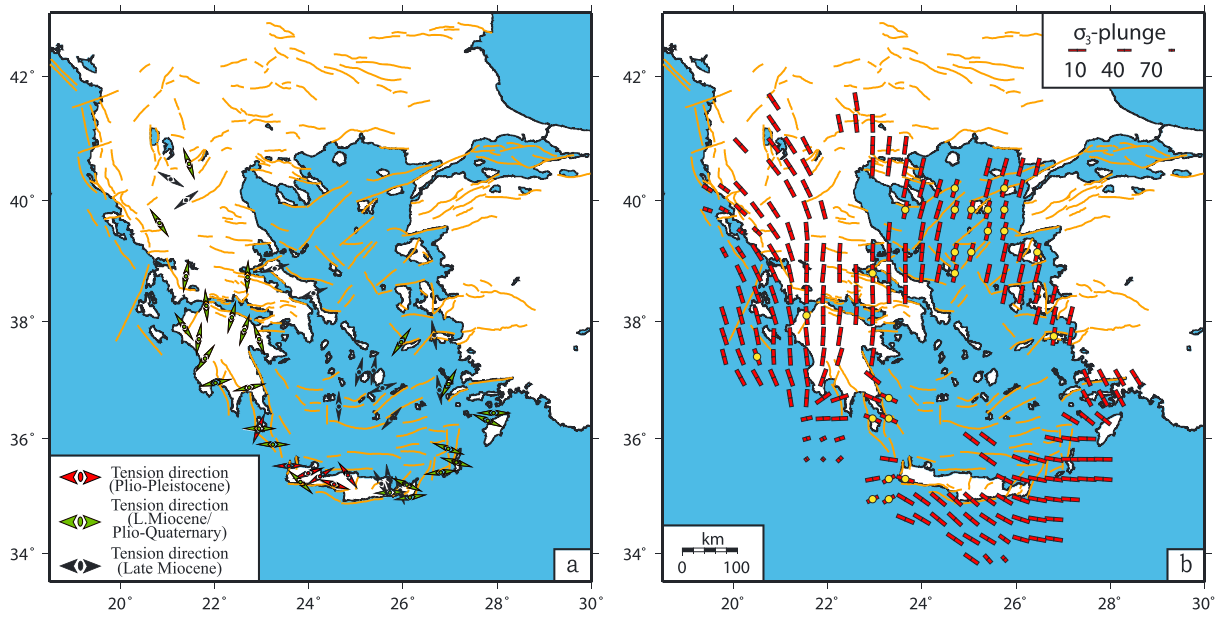

Figure 6. (a) Paleostress estimates of tension orientations as determined for mainland Greece and the southern Aegean by *Doutsos and Kokkalas* [2001] overlaid on active faults traces in the Greek region adopted from the database of *Caputo and Pavlides* [2013] and (b) orientations of minimum stress axes determined in this study from stress inversion of earthquake focal mechanisms. All other symbols are the same as in Figure 5.

an angle of 45° with them. We confirm that this relationship holds also for the minimum principal stress axes, as can be seen in the case of the NAF and its branches in the northern Aegean, normal faults in mainland Greece, and the KTF in western Greece (cf. Figure 6b). This reinforces the argument that crustal deformation in the Greek region is accommodated by slip on preexisting faults with presumably low effective coefficients of friction.

The derivation of the crustal principal stress axes also gives us the opportunity to decipher for each node of our grid the dominant faulting type and investigate how transitions occur between different types. Following

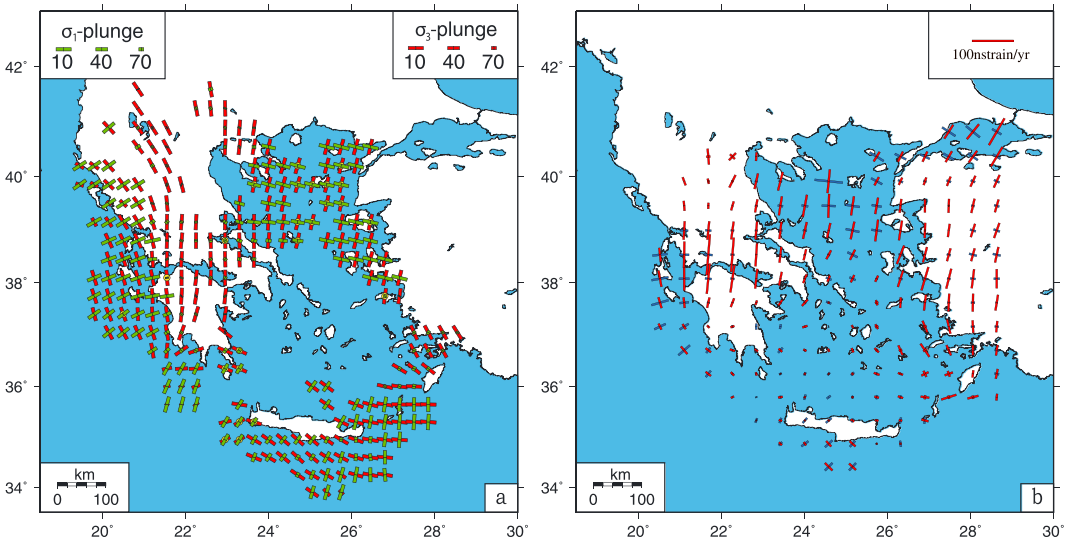

Figure 7. Comparison of principal maximum/minimum stress and strain axes adopted from the study of *Floyd et al*. [2010]. (a) The symbols of stress axes are the same as in Figure 5. (b) The red lines indicate the extensional strain axes, while the blue lines represent the compressional strain axes. The length of each strain axis gives the value of strain rate if compared to the benchmark line at the top right-hand corner of the plot.

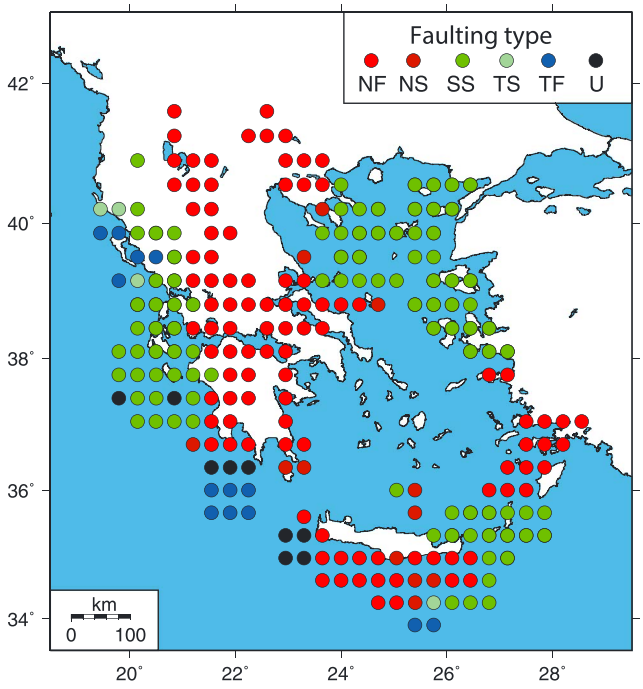

Figure 8. Map showing the faulting regime of each node determined after considering the azimuths and plunges of the three principal stress axes following *Zoback* [1992]. NF: normal faulting, NS: normal and strike slip, SS: strike slip, TS: thrust and strike slip, TF: thrust faulting, U: unknown type of faulting.

the scheme suggested by *Zoback* [1992] we use the azimuth and plunge of the stress axes in order to group each node into six different faulting types (normal, thrust, strike-slip, unknown faulting, and mixed types), and results are shown in Figure 8. Normal faulting dominates in mainland Greece, the largest part of Peloponnese, southern Crete, the Gökova graben, and Rhodes Island. Thrust faulting is limited in three areas: NW Epirus owing to continental collision, offshore SW Peloponnese, and south of Crete owing to stresses along the subduction interface. Strike-slip faulting extends in the northern Aegean covering the area of the different NAF branches, KTF, and the largest part of western Greece, as well as offshore eastern Crete and Karpathos Island. Unknown type of faulting occurs in SW Peloponnese and western Crete that were found to exhibit either stress heterogeneity or spatial variations of stress (see supporting information) and in two nodes south of Zakynthos. Transition from thrust faulting in Epirus to normal faulting in NW Greece seems to occur within a distance of less than 100 km, confirming the earlier observations of *Hatzfeld et al.* [1990]. Similarly, the transition from strike-slip to normal faulting in the northern and SE Aegean occurs within a distance of some tens of kilometers, even though strike-slip faulting affects not just a narrow strip around the main segments of NAF or KTF but areas much wider than the trace of each fault.

5. Conclusions

We selected 1614 earthquake focal mechanisms derived from waveform inversion for the purpose of inverting them and determine principal axes of crustal stress in Greece. Our approach is novel for this region in two respects: first for the amount and quality of data utilized and second for obtaining a stress field that retains only the degree of spatial variation that is strongly required by the data. The main conclusions of this work can be summarized as follows:

1. The minimum principal stress axes rotate clockwise and counterclockwise in SW and SE Aegean, respectively, confirming earlier analogue and geomechanical-numerical models that the extension in the Aegean occurs in response to slab rollback and gravitational spreading of the upper plate lithosphere.
2. There is a very good agreement between the azimuths of the horizontal principal stress and horizontal principal strain axes derived from GPS observations. This indicates a rather elastic behavior of the crust in the Greek region. Furthermore, the orientation of the minimum principal stress axes relative to the major normal and strike-slip faults imply close to Andersonian style of faulting.
3. Transitions from one faulting type to another seem to occur within narrow zones of some tens of kilometers. It is also observed that strike-slip faulting affects not only a narrow strip around the main segments of NAF or KTF but also areas much wider than the trace of each fault.
4. Comparisons with previous stress inversion studies, as well as geological observations, show very good agreement with the results presented here. Any differences can be attributed either to the limited amount of data of previous works or to the use of microearthquakes for stress inversion, which led to the derivation of the local rather than the regional stresses.

Acknowledgments

This research has been funded by Taiwan's MOST (under grant 104-2911-I-008-503-MY2) and Germany's DAAD (under grant 920217) agencies. The authors of this work declare no financial conflicts of interests. The focal mechanism solutions used in this study can be found in the GCMT database (http://www.globalcmt.org), the RCMT database (http://www.bo.ingv.it/RCMT), the database of the National Observatory of Athens Institute of Geodynamics (http://bbnet.gein.noa.gr), and the published literature cited in the main body of the paper or the supporting information. We would like to express our gratitude to all the people that help maintain the aforementioned databases. We would like to thank the Editor-in-Chief Martha Savage and Associate Editor Honn Kao for handling our manuscript, as well as Mimmo Palano and Vaclav Vavryčuk for their constructive reviews.

References

Angelier, J. (2002), Inversion of earthquake focal mechanisms to obtain the seismotectonic stress IV—A new method free of choice among nodal lines, *Geophys. J. Int.*, *150*, 588–609.

Angelier, J., N. Lyberis, X. Le Pichon, and P. Huchon (1982), The tectonic development of the Hellenic trench and Sea of Crete: A synthesis, *Tectonophysics*, *86*, 159–196.

Baker, C., D. Hatzfeld, H. Lyon-Caen, E. Papadimitriou, and A. Rigo (1997), Earthquake mechanisms of the Adriatic Sea and western Greece: Implications for the oceanic subduction-continental collision transition, *Geophys. J. Int.*, *131*, 559–594.

Becker, D., T. Meier, M. Rische, M. Bohnhoff, and H.-P. Harjes (2006), Spatio-temporal microseismicity in the Cretan region, *Tectonophysics*, *423*, 3–16, doi:10.1016/j.tecto.2006.03.022.

Becker, D., T. Meier, M. Bohnhoff, and H.-P. Harjes (2010), Seismicity at the convergent plate boundary offshore Crete, Greece, observed by an amphibian network, *J. Seismol.*, *14*, 369–392, doi:10.1007/s10950-009-9170-2.

Benetatos, C., A. Kiratzi, C. Papazachos, and G. Karakaisis (2004), Focal mechanisms of shallow and intermediate depth earthquakes along the Hellenic arc, *J. Geodyn.*, *37*(2), 253–296, doi:10.1016/j.jog.2004.02.002.

Bohnhoff, M., H.-P. Harjes, and T. Meier (2005), Deformation and stress regimes in the Hellenic subduction zone from focal mechanisms, *J. Seismol.*, *9*, 341–366.

Caputo R., and Pavlides S. (2013), The Greek Database of Seismogenic Sources (GreDaSS), Version 2.0.0: A compilation of potential seismogenic sources ($M_w > 5.5$) in the Aegean region, doi:10.15160/unife/gredass/0200. [Available at http://gredass.unife.it/.]

Célérier, B. (2010), Remarks on the relationship between the tectonic regime, the rake of the slip vectors, the dip of the nodal planes, and the plunges of the *P*, *B*, *T* axes of earthquake focal mechanisms, *Tectonophysics*, *482*, 1042–1049, doi:10.1016/j.tecto.2009.1003.1006.

Chamot-Rooke, N., and Dotmed Working Group (2005), *DOTMED-Deep Offshore Tectonics of the Mediterranean: A Synthesis of Deep Marine Data in Eastern Mediterranean*, *Mem. Soc. Geol. Fr.*, vol. 177, pp. 1–64, Société Géologique de France, Paris.

Chang, C.-P., T.-Y. Chang, J. Angelier, H. Kao, J.-C. Lee, and S.-B. Yu (2003), Strain and stress field in Taiwan oblique convergent system: Constraints from GPS observation and tectonic data, *Earth Planet. Sci. Lett.*, *214*, 115–127, doi:10.1016/S0012-821X(03)00360-1.

Chatzipetros, A., A. Kiratzi, N. Zouros, and S. Pavlides (2013), Active faulting in the north-eastern Aegean Sea islands, *Tectonophysics*, *597–598*, 106–122, doi:10.0116/j.tecto.2012.11.026.

Chousianitis, K., A. Ganas, and C. P. Evangelidis (2015), Strain and rotation rate patterns of the mainland Greece from continuous GPS data and comparison between seismic and geodetic moment release, *J. Geophys. Res. Solid Earth*, *120*, 3909–3931, doi:10.1002/2014JB011762.

Clément, C., A. Hirn, P. Charvis, M. Sachpazi, and F. Marnelis (2000), Seismic structure and the active Hellenic subduction in the Ionian Islands, *Tectonophysics*, *329*, 141–156.

Copley, A., F. Boait, J. Hollingsworth, J. Jackson, and D. McKenzie (2009), Subparallel thrust and normal faulting in Albania and the roles of gravitational potential energy and rheology contrasts in mountain belts, *J. Geophys. Res.*, *114*, B05407, doi:10.1029/2008JB005931.

Doutsos, T., and S. Kokkalas (2001), Stress and deformation patterns in the Aegean region, *J. Geodyn.*, *23*, 455–472.

Ekström, G., M. Nettles, and A. Dziewonski (2012), The Global CMT project 2004–2010: Centroid-moment tensors for 13,017 earthquakes, *Phys. Earth Planet. Inter.*, *200–201*, 1–9, doi:10.1016/j.pepi.2012.04.002.

England, P. (2003), The alignment of earthquake *T*-axes with the principal axes of geodetic strain in the Aegean region, *Turk. J. Earth Sci.*, *12*, 47–53.

Evangelidis, C. P. (2015), Imaging supershear rupture for the 2014 M_w 6.9 northern Aegean earthquake by backprojection of strong motion waveforms, *Geophys. Res. Lett.*, *42*, 307–315, doi:10.1002/2014GL062513.

Evangelidis, C. P., K. I. Konstantinou, N. S. Melis, M. Charalambakis, and G. N. Stavrakakis (2008), Waveform relocation and focal mechanism analysis of an earthquake swarm in Trichonis Lake, western Greece, *Bull. Seismol. Soc. Am.*, *98*, 804–811, doi:10.1785/0120070185.

Ferentinos, G., M. Brooks, and T. Doutsos (1985), Quaternary tectonics in the Gulf of Patras, western Greece, *J. Struct. Geol.*, *7*, 713–717.

Feuillet, N. (2013), The 2011–2012 unrest at Santorini rift: Stress interaction between active faulting and volcanism, *Geophys. Res. Lett.*, *40*, 3532–3537, doi:10.1002/grl.50516.

Flerit, F., R. Armijio, G. King, and B. Meyer (2004), The mechanical interaction between the propagating North Anatolian Fault and the back-arc extension in the Aegean, *Earth Planet. Sci. Lett.*, *224*, 347–362, doi:10.1016/j.epsl.2004.05.028.

Floyd, M. A., et al. (2010), A new velocity field for Greece: Implications for the kinematics and dynamics of the Aegean, *J. Geophys. Res.*, *115*, B10403, doi:10.1029/2009JB007040.

Friederich, W., A. Brüstle, L. Küpperkoch, T. Meier, and S. Lamara (2014), Focal mechanisms in the southern Aegean from temporary seismic networks—Implications for the regional stress field and ongoing deformation process, *Solid Earth*, *5*(1), 275–297, doi:10.5194/se-5-275-2014.

Frohlich, C., and S. D. Davis (1999), How well are well-constrained *T*, *B* and *P* axes in moment tensor catalogs?, *J. Geophys. Res.*, *104*, 4901–4910, doi:10.1029/1998JB900071.

Fuchs, K., and B. Müller (2001), World stress map of the Earth: A key to tectonic processes and technological applications, *Naturwissenschaften*, *88*, 357–371.

Ganas, A., G. Drakatos, S. B. Pavlides, G. N. Stavrakakis, M. Ziazia, E. Sokos, and V. K. Karastathis (2005), The 2001 $M_w = 6.4$ Skyros earthquake, conjugate strike-slip faulting and spatial variation in stress within the central Aegean Sea, *J. Geodyn.*, *39*, 61–77, doi:10.1016/j.jog.2004.09.001.

Gautier, P., J.-P. Brun, R. Moriceau, D. Sokoutis, J. Martinod, and L. Jolivet (1999), Timing, kinematics and cause of Aegean extension: A scenario based on a comparison with simple analogue experiments, *Tectonophysics*, *315*, 31–72.

Gephart, J. W., and D. W. Forsyth (1984), An improved method for determining the regional stress tensor using earthquake focal mechanism data: Application to the San Fernando earthquake sequence, *J. Geophys. Res.*, *89*, 9305–9320, doi:10.1029/JB089iB11p09305.

Giannopoulos, D., E. Sokos, K. I. Konstantinou, and G.-A. Tselentis (2015), Shear wave splitting and V_p/V_s variations before and after the Efpalio earthquake sequence, western Gulf of Corinth, Greece, *Geophys. J. Int.*, *200*, 1436–1448, doi:10.1093/gji/ggu467.

Goldsworthy, M., J. Jackson, and J. Haines (2002), The continuity of active faults systems in Greece, *Geophys. J. Int.*, *148*, 596–618.

Hardebeck, J. L., and E. Haukson (2001), Stress orientations obtained from earthquake focal mechanisms: What are appropriate uncertainty estimates?, *Bull. Seismol. Soc. Am.*, *91*, 250–262.

Hardebeck, J. L., and A. J. Michael (2006), Damped regional-scale stress inversions: Methodology and examples for Southern California and the Coalinga aftershock sequence, *J. Geophys. Res.*, *111*, B11310, doi:10.1029/2005JB004144.

Hatzfeld, D., G. Pedotti, P. Hatzidimitriou, and K. Makropoulos (1990), The strain pattern in the western Hellenic arc from a microearthquake survey, *Geophys. J. Int.*, *101*, 181–202.

Hatzfeld, D., I. Kassaras, D. Panagiotopoulos, D. Amorese, K. Makropoulos, G. Karakaisis, and O. Coutant (1995), Microseismicity and strain pattern in northwestern Greece, *Tectonics*, *14*, 773–785, doi:10.1029/95TC00839.
Hatzfeld, D., J. Martinod, G. Bastet, and P. Gautier (1997), An analog experiment for the Aegean to describe the contribution of gravitational potential energy, *J. Geophys. Res.*, *102*, 649–659, doi:10.1029/96JB02594.
Hatzfeld, D., M. Ziazia, D. Kemenetzidou, P. Hatzidimitriou, D. Panagiotopoulos, K. Makropoulos, P. Papadimitriou, and A. Deschamps (1999), Microseismicity and focal mechanisms at the western termination of the North Anatolian Fault and their implications for continental tectonics, *Geophys. J. Int.*, *137*, 891–908.
Hatzfeld, D., V. Karakostas, M. Ziazia, I. Kassaras, E. Papadimitriou, K. Makropoulos, N. Voulgaris, and C. Papaioannou (2000), Microseismicity and faulting geometry in the Gulf of Corinth (Greece), *Geophys. J. Int.*, *141*, 438–456.
Heidbach, O., J. Reinecker, M. Tingay, B. Müller, B. Spencer, K. Fuchs, and F. Wenzel (2007), Plate boundary forces are not enough: Second- and third-order stress patterns highlighted in the World Stress Map database, *Tectonics*, *26*, TC6014, doi:10.1029/200TC002133.
Heidbach, O., M. Tingay, A. Barth, J. Reinecker, D. Kurfeß, and B. Müller (2010), Global crustal stress pattern on the World Stress Map database release 2008, *Tectonophysics*, *482*, 3–15, doi:10.1016/j.tecto.2009.07.023.
Helffrich, G. R. (1997), How good are routinely determined focal mechanisms? Empirical statistics based on a comparison of Harvard, USGS and ERI moment tensors, *Geophys. J. Int.*, *131*, 741–750, doi:10.1111/j.1365-246X.1997.tb06609.x.
Hergert T., and O. Heidbach (2011), Geomechanical model of the Marmara Sea region-II. 3-D contemporary background stress field, *Geophys. J. Int.*, *185*, 1090–1102.
Herrmann, R. B., and C. J. Ammon (2002), Computer programs in seismology–source inversions: User's manual, report St Louis University, St. Louis, Mo.
Hollenstein, C., M. D. Müller, A. Geiger, and H.-G. Kahle (2008), Crustal motion and deformation in Greece from a decade of GPS measurements, 1993–2003, *Tectonophysics*, *449*(1), 17–40, doi:10.1016/j.tecto.2007.12.006.
Huguen, C., J. Mascle, E. Chaumillion, J. M. Woodside, J. Benkhelil, and A. Volkonskaia (2001), Deformation of the eastern Mediterranean Ridge and surroundings from combined swath mapping and seismic reflection profiling, *Tectonophysics*, *343*, 21–47.
Ickrath, M., M. Bohnhoff, F. Bulut, and G. Dresen (2014), Stress rotation and recover in conjunction with the 1999 Izmit M_w 7.4 earthquake, *Geophys. J. Int.*, *196*, 951–956, doi:10.1093/gji/ggt409.
Jolivet, L., et al. (2013), Aegean tectonics: Strain localisation, slab tearing and trench retreat, *Tectonophysics*, *597–598*, 1–33, doi:10.1016/j.tecto.2012.06.011.
Jost, M. L., O. Knabenbauer, J. Cheng, and H.-P. Harjes (2002), Fault plane solutions of microearthquakes and small events in the Hellenic arc, *Tectonophysics*, *356*, 87–114.
Kagan, Y. Y. (1991), 3-D rotation of double-couple earthquake sources, *Geophys. J. Int.*, *106*, 709–716.
Kagan, Y. Y. (2003), Accuracy of modern global earthquake catalogs, *Phys. Earth Planet. Inter.*, *135*(2–3), 173–209, doi:10.1016/S0031-9201(02)00214-5.
Keiding, M., B. Lund, and T. Arnadottir (2009), Earthquakes, stress, and strain along an obliquely divergent plate boundary: Reykjanes peninsula, southwest Iceland, *J. Geophys. Res.*, *114*, B09306, doi:10.1029/2008JB006253.
Kiratzi, A. (2002), Stress tensor inversions along the westernmost North Anatolian Fault Zone and its continuation into the North Aegean Sea, *Geophys. J. Int.*, *151*, 360–376.
Kiratzi, A. (2010), The 24 May 2009 M_w5.2 earthquake sequence near Lake Doirani (FYROM-Greek borders): Focal mechanisms and slip model using empirical source time functions inversion, *Tectonophysics*, *490*, 115–122, doi:10.1016/j.tecto.2010.04.35.
Kiratzi, A. (2013), The January 2012 earthquake sequence in the Cretan Basin, south of the Hellenic volcanic arc: Focal mechanisms, rupture directivity and slip models, *Tectonophysics*, *586*, 160–172, doi:10.1016/j.tecto.2012.11.019.
Kokinou, E., E. Kamberis, A. Vafidis, D. Monopolis, G. Ananiadis, and A. Zelelidis (2005), Deep seismic reflection data from offshore western Greece: A new crustal model for the Ionian Sea, *J. Pet. Geol.*, *28*, 185–202.
Kokinou, E., E. Papadimitriou, V. Karakostas, E. Kamberis, and F. Vallianatos (2006), The Kefalonia Transform Zone (offshore western Greece) with special emphasis to its prolongation towards the Ionian abyssal plain, *Mar. Geophys. Res.*, *27*, 241–252, doi:10.1007/s11001-006-9005-2.
Kokinou, E., A. Tiago, and K. Evangelos (2012), Structural decoupling in a convergent forearc setting (southern Crete, eastern Mediterranean), *Geol. Soc. Am. Bull.*, *124*, 1352–1364.
Konstantinou, K. I. (2014), Moment magnitude-rupture area scaling and stress-drop variations for earthquakes in the Mediterranean region, *Bull. Seismol. Soc. Am.*, *104*, 2378–2386, doi:10.1785/0120140062.
Konstantinou, K. I., N. S. Melis, S.-J. Lee, C. P. Evangelidis, and K. Boukouras (2009), Rupture process and aftershocks relocation of the 8 June 2008 M_w 6.4 NW Peloponnese, western Greece, *Bull. Seismol. Soc. Am.*, *99*, 3374–3389, doi:10.1785/0120080301.
Konstantinou, K. I., N. S. Melis, and K. Boukouras (2010), Routine regional moment tensor inversion for earthquakes in the Greek region: The National Observatory of Athens (NOA) database (2001–2006), *Seismol. Res. Lett.*, *81*, 738–748, doi:10.1785/gssrl.81.5.738.
Konstantinou, K. I., C. P. Evangelidis, and N. S. Melis (2011), The 8 June 2008 (M_w 6.4) earthquake in northwest Peloponnese: A case of fault reactivation in an overpressured lower crust?, *Bull. Seismol. Soc. Am.*, *101*, 438–445, doi:10.1785/0120100074.
Konstantinou, K. I., C. P. Evangelidis, W. T. Liang, N. S. Melis, and I. Kalogeras (2013), Seismicity, V_p/V_s and shear wave anisotropy variations during the 2011 unrest at Santorini caldera, southern Aegean, *J. Volcanol. Geotherm. Res.*, *267*, 57–67, doi:10.1016/j.jvolgeores.2013.10.001.
Koukouvelas, I. K., and A. Aydin (2002), Fault structure and related basins of the North Aegean Sea and its surroundings, *Tectonics*, *21*(5), 1046, doi:10.1029/2001TC901037.
Kreemer, C., and N. Chamot-Rooke (2004), Contemporary kinematics of the southern Aegean and the Mediterranean Ridge, *Geophys. J. Int.*, *157*, 1377–1392, doi:10.1111/j.1365-246X.2004.02270.x.
Kreemer, C., N. Chamot-Rooke, and X. Le Pichon (2004), Constraints on the evolution and vertical coherency of deformation in the Northern Aegean from a comparison of geodetic, geologic and seismologic data, *Earth Planet. Sci. Lett.*, *225*, 329–346, doi:10.1016/j.epsl.2004.06.018.
Laigle, M., A. Hirn, M. Sachpazi, and N. Rousos (2000), North Aegean crustal deformation: An active fault imaged to 10 km depth by reflection seismic data, *Geology*, *28*, 71–74.
Laigle, M., A. Hirn, M. Sachpazi, and C. Clément (2002), Seismic coupling and structure of the Hellenic subduction zone in the Ionian Islands region, *Earth Planet. Sci. Lett.*, *200*, 243–253.
Lyon-Caen, H., et al. (1988), The 1986 Kalamata (south Peloponnese) earthquake: Detailed study of a normal fault, evidences for east-west extension in the Hellenic arc, *J. Geophys. Res.*, *93*, 14,967–15,000, doi:10.1029/JB093iB12p14967.
Martinez-Garzón, P., M. Bohnhoff, G. Kwiatek, and G. Dresen (2013), Stress tensor changes related to fluid injection at the Geysers geothermal field, California, *Geophys. Res. Lett.*, *40*, 2596–2601, doi:10.1002/grl.50438.

Martinod, J., D. Hatzfeld, J.-P. Brun, J.-P. Davy, and P. Gautier (2000), Continental collision, gravity spreading, and kinematics of Aegea and Anatolia, *Tectonics*, *19*, 290–299, doi:10.1029/1999TC900061.
Maury, J., F. H. Cornet, and L. Dorbath (2013), A review of methods for determining stress fields from earthquake focal mechanisms: Application to the Sierentz 1980 seismic crisis (Upper Rhine graben), *Bull. Soc. Geol. Fr.*, *184*, 319–334.
McClusky, S., et al. (2000), Global positioning system constraints on plate kinematic and dynamics in the eastern Mediterranean and Caucasus, *J. Geophys. Res.*, *105*, 5695–5719, doi:10.1029/1999JB900351.
McKenzie, D. (1969), The relation between fault plane solutions for earthquakes and the directions of the principal stresses, *Bull. Seismol. Soc. Am.*, *59*, 591–601.
Meier, T., M. Rische, B. Endrun, A. Vafidis, and H.-P. Harjes (2004), Seismicity of the Hellenic subduction zone in the area of the western and central Crete observed by temporary local seismic networks, *Tectonophysics*, *383*, 149–169, doi:10.1016/j.tecto.2004.02.004.
Meijer, P. T., and M. J. R. Wortel (1997), Present-day dynamics of the Aegean region: A model analysis of the horizontal pattern of stress and deformation, *Tectonics*, *16*, 879–895, doi:10.1029/97TC02004.
Melis, N. S., and G.-A. Tselentis (1998), 3-D P-wave velocity structure in western Greece determined from tomography using earthquake data recorded at the University of Patras Seismic Network (PATNET), *Pure Appl. Geophys.*, *152*, 329–348.
Michael, A. J. (1984), Determination of stress from slip data: Faults and folds, *J. Geophys. Res.*, *89*, 11,517–11,526, doi:10.1029/JB089iB13p11517.
Michael, A. J. (1987), Use of focal mechanisms to determine stress: A control study, *J. Geophys. Res.*, *92*, 357–368, doi:10.1029/JB092iB01p00357.
Mouslopoulou, V., V. Saltogianni, M. Gianniou, and S. Stiros (2014), Geodetic evidence for tectonic activity on the Strymon Fault System, northeast Greece, *Tectonophysics*, *633*, 246–255.
Mouslopoulou, V., A. Nicol, J. Begg, O. Oncken, and M. Moreno (2015), Clusters of megaearthquakes on upper plate faults control the eastern Mediterranean hazard, *Geophys. Res. Lett.*, *42*, 10,282–10,289, doi:10.1002/2015GL066371.
Nyst, M., and W. Thatcher (2004), New constraints on the active tectonic deformation of the Aegean, *J. Geophys. Res.*, *109*, B11406, doi:10.1029/2003JB002830.
Palano, M. (2015), On the present-day crustal stress, strain-rate fields and mantle anisotropy pattern of Italy, *Geophys. J. Int.*, *200*, 967–983, doi:10.1093/gji/ggu451.
Papanikolaou, D., M. Alexandri, P. Nomikou, and D. Ballas (2002), Morphotectonic structure of the western part of the North Aegean Basin based on swath bathymetry, *Mar. Geol.*, *190*, 465–492.
Papazachos, B. C., and K. Papazachou (2003), *The Earthquakes of Greece*, Ziti Editions, Thessaloniki.
Papazachos, B. C., V. G. Karakostas, C. B. Papazachos, and E. M. Scordilis (2000), The geometry of the Wadati-Benioff zone and lithospheric kinematics in the Hellenic arc, *Tectonophysics*, *319*, 275–300.
Pierdominici, S., and O. Heidbach (2012), Stress field of Italy—Mean stress orientation at different depths and wavelength of the stress pattern, *Tectonophysics*, *532–535*, 301–311, doi:10.1016/j.tecto.2012.02.018.
Pondrelli, S., S. Salimbeni, A. Morelli, G. Ekström, L. Postpischl, G. Vannucci, and E. Boschi (2011), European-Mediterranean Regional Centroid Moment Tensor catalog: Solutions for 2005–2008, *Phys. Earth Planet. Inter.*, *185*, 74–81, doi:10.1016/j.pepi.2011.01.007.
Reilinger, R., S. McClusky, D. Paradisis, S. Ergintav, and P. Vernant (2010), Geodetic constraints on the tectonic evolution of the Aegean region and strain accumulation along the Hellenic subduction zone, *Tectonophysics*, *488*, 22–30, doi:10.1016/j.tecto.2009.05.027.
Richardson, R. M. (1992), Ridge forces, absolute plate motions and the intraplate stress field, *J. Geophys. Res.*, *97*, 11,739–11,748, doi:10.1029/91JB00475.
Rigo, A., H. Lyon-Caen, R. Armijo, A. Deschamps, D. Hatzfeld, K. Makropoulos, P. Papadimitriou, and I. Kassaras (1996), A microseismic study in the western part of the Gulf of Corinth (Greece): Implications for large-scale normal faulting mechanisms, *Geophys. J. Int.*, *126*, 663–688.
Rontogianni, S. (2010), Comparison of geodetic and seismic strain rates in Greece by using a uniform processing approach to campaign GPS measurements over the interval 1994–2000, *J. Geodyn.*, *50*, 381–399, doi:10.1016/j.jog.2010.04.008.
Roumelioti, Z., C. Benetatos, and A. Kiratzi (2009), The 14 February 2008 earthquake (*M*6.7) sequence offshore south Peloponnese (Greece): Source models of the three strongest events, *Tectonophysics*, *471*, 272–284, doi:10.1016/j.tecto.2009.02.28.
Saatçilar, R., S. Ergintav, E. Demirbag, and S. Inan (1999), Character of active faulting in the North Aegean Sea, *Mar. Geol.*, *160*, 339–353.
Saltogianni, V., S. C. Stiros, A. V. Newman, K. Flanagan, and F. Moschas (2014), Time-space modeling of the dynamics of Santorini volcano (Greece) during the 2011–2012 unrest, *J. Geophys. Res. Solid Earth*, *119*, 8517–8537, doi:10.1002/2014JB011409.
Segall, P., and S. D. Fitzgerald (1998), A note on induced stress changes in hydrocarbon and geothermal reservoirs, *Tectonophysics*, *289*, 117–128.
Serpetsidaki, A., G.-A. Tselentis, N. Martakis, and E. Sokos (2012), Seismicity and seismotectonics study in southwestern Albania using a local dense seismic network, *Bull. Seismol. Soc. Am.*, *102*, 2090–2097, doi:10.1785/0120110139.
Serpetsidaki, A., P. Elias, M. Ilieva, P. Bernard, P. Briole, A. Deschamps, S. Lambotte, H. Lyon-Caen, E. Sokos, and G.-A. Tselentis (2014), New constraints from seismology and geodesy on the $M_w = 6.4$ 2008 Movri (Greece) earthquake: Evidence for a growing strike-slip fault system, *Geophys. J. Int.*, *198*, 1373–1386, doi:10.1093/gji/ggu212.
Shaw, B., and J. Jackson (2010), Earthquake mechanisms and active tectonics of the Hellenic subduction zone, *Geophys. J. Int.*, *181*, 966–984, doi:10.1111/j.1365-246X.2010.04551.x.
Shaw, B., N. N. Ambraseys, P. C. England, M. A. Floyd, G. J. Gorman, T. F. G. Higham, J. A. Jackson, J.-M. Nocquet, C. C. Pain, and M. D. Piggott (2008), Eastern Mediterranean tectonics and tsunami hazard inferred from the AD 365 earthquake, *Nat. Geosci.*, *1*, 268–276, doi:10.0138/ngeo151.
Sodoudi, F., et al. (2006), Lithospheric structure of the Aegean obtained from *P* and *S* receiver functions, *J. Geophys. Res.*, *111*, B12307, doi:10.1029/2005JB003932.
Sokos, E. N., and J. Zahradnik (2008), ISOLA: A FORTRAN code and a MATLAB GUI to perform multiple-point source inversion of seismic data, *Comput. Geosci.*, *34*, 967–977, doi:10.1016/j.cageo.2007.07.005.
Sperner, B., B. Müller, O. Heidbach, D. Delvaux, J. Reinecker, and K. Fuchs (2003), Tectonic stress in the Earth's crust: Advances in the World Stress Map project, in *New Insights in Structural Interpretation and Modeling*, *Geol. Soc. Spec. Publ.*, vol. 212, edited by D. A. Nieuwland, pp. 101–116.
Stein, R. S. (1999), The role of stress transfer in earthquake occurrence, *Nature*, *402*, 605–609.
Stiros, S. (2010), The 8.5+ magnitude, AD 365 earthquake in Crete: Coastal uplift, topography changes and archaeological and historical signature, *Quat. Int.*, *216*, 54–63.
Tingay, M., B. Müller, J. Reinecker, O. Heidbach, F. Wenzel, and P. Fieckerstein (2005), Understanding tectonic stress in the oil patch: The World Stress Map project, *Leading Edge*, *24*, 1276–1282.

Tirel, C., F. Gueydan, C. Tiberi, and J.-P. Brun (2004), Aegean crustal thickness inferred from gravity inversion: Geodynamic implications, *Earth Planet. Sci. Lett.*, *228*, 267–280, doi:10.1016/j.epsl.2004.10.023.

Tselentis, G.-A., E. Sokos, N. Martakis, and A. Serpetsidaki (2006), Seismicity and seismotectonics in Epirus, western Greece: Results from a microearthquake survey, *Bull. Seismol. Soc. Am.*, *96*, 1706–1717, doi:10.1785/0120020086.

Vavryčuk, V. (2014), Iterative joint inversion for stress and fault orientations from focal mechanisms, *Geophys. J. Int.*, *199*, 69–77, doi:10.1093/gji/ggu224.

Wu, W.-N., H. Kao, S.-K. Hsu, C.-L. Lo, and H.-W. Chen (2010), Spatial distribution of the crustal stress field along the Ryukyu-Taiwan-Luzon convergent boundary, *J. Geophys. Res.*, *115*, B11401, doi:10.1029/2009JB007080.

Yang, W., and E. Hauksson (2013), The tectonic crustal stress field and style of faulting along the Pacific North America Plate boundary in Southern California, *Geophys. J. Int.*, *194*, 100–117, doi:10.1093/gji/ggt113.

Yoshida, K., A. Hasegawa, and T. Okada (2015), Spatial variation of stress orientations in NE Japan revealed by dense seismic observations, *Tectonophysics*, *647–648*, 63–72, doi:10.1016/j.tecto.2015.02.013.

Zoback, M. (2010), *Reservoir Geomechanics*, 449 pp., Cambridge Univ. Press, Cambridge, U. K.

Zoback, M. L. (1992), First- and second-order patterns of stress in the lithosphere: The World Stress Map project, *J. Geophys. Res.*, *97*, 11,703–11,728, doi:10.1029/92JB00132.

Zoback, M. L., et al. (1989), Global patterns of tectonic stress, *Nature*, *341*, 291–298.